Study of the measurement of the τ lepton anomalous magnetic moment in high energy lead-lead collisions at the LHC

Monica Verducci,* Chiara Roda,† and Vincenzo Cavasinni‡

Dipartimento di Fisica, Università di Pisa and Istituto Nazionale di Fisica Nucleare, Sezione di Pisa, I-56127 Pisa, Italy

Natascia Vignaroli§

Dipartimento di Fisica, Università di Napoli and Istituto Nazionale di Fisica Nucleare, Sezione di Napoli, I-80126 Napoli, Italy and Dipartimento di Matematica e Fisica, Università del Salento, and Istituto Nazionale di Fisica Nucleare, Sezione di Lecce, I-73100 Lecce, Italy

(Received 6 February 2024; accepted 30 July 2024; published 6 September 2024)

The τ lepton anomalous magnetic moment $a_\tau = \frac{g_\tau - 2}{2}$ was measured, so far, with a precision of only several percents, despite its high sensitivity to physics beyond the Standard Model such as compositeness or supersymmetry. A new study is presented to improve the sensitivity of the a_τ measurement with photon-photon interactions from ultraperipheral lead-lead collisions at the LHC. The theoretical approach used in this work is based on an effective Lagrangian and on a photon flux implemented in the MadGraph5 Monte Carlo simulation. Using a multivariate analysis to discriminate the signal from the background processes, a sensitivity to the anomalous magnetic moment $a_\tau = 0^{-0.019}_{+0.015}$ is obtained at 95% confidence level with a dataset corresponding to an integrated luminosity of 2 nb^{-1} of lead-lead collisions and assuming a conservative 10% systematic uncorrelated uncertainty for signal and background. The present results using multivariate analysis are compared to similar results obtained using sequential cuts, as done in previous measurements, showing an improvement of about 35% in the sensitivity to a_τ.

DOI: 10.1103/PhysRevD.110.052001

I. INTRODUCTION

The anomalous magnetic moment of elementary particles (leptons and quarks) is defined as $a_{l,q} = \frac{g_{l,q} - 2}{2}$, where Dirac theory of the QED implies at the classical level $g_{l,q} = 2$. The measurement of $a_{l,q}$ is today one of most powerful tools to test the validity of the Standard Model (SM) theory that, despite its indisputable success, cannot be a complete theory. There are, in fact, several unresolved questions not addressed by the SM such as, for example, the existence of "dark matter," estimated to be about 5 times more abundant than the ordinary matter. Precise measurements of the elementary particles' magnetic moment and its comparison with the Standard Model predictions could indicate the existence of new interactions and particles that could shed light also on the nature of the dark matter and on the problems of the naturalness and fine-tuning of the Higgs boson mass.

Extensive research of new physics, new particles, and deviations from the SM predictions have been carried out at the LHC, but no clear hints of the existence of new phenomena have emerged from the data collected so far. The LHC run restarted in 2022 with the LHC performances improved both in energy and luminosity and searches of new particles will continue, but the limited energy/mass at which they could be produced and detected will remain to be on the order of 1 TeV.

A discrepancy between the values of $a_{l,q}$ predicted by the SM and the measured ones could provide important clues to anticipate both the nature and the mass of the new phenomena, suggesting also the energy regime at which a direct production of the new particles responsible for these discrepancies could be expected. This, of course, would be possible if, on one hand, a precise calculation is provided of the SM predictions, and, on the other hand, accurate measurements of the anomalous $a_{l,q}$ will be performed for the three charged leptons.

For an accurate prediction of $a_{l,q}$ within the SM it is crucial to have a precise evaluation of high order electromagnetic (QED) and weak and strong (QCD) interaction

*Contact author: monica.verducci@cern.ch
†Contact author: chiara.roda@cern.ch
‡Contact author: vincenzo.cavasinni@cern.ch
§Contact author: natascia.vignaroli@unisalento.it

corrections. These QED corrections were first calculated for the electron in the seminal paper by Schwinger [1] to be $a_e = \frac{\alpha}{2\pi} = 0.001162$, where α is the fine structure constant.

The QCD corrections are difficult to calculate in an energy range where no perturbation development is applicable and corrections should rely on experimental cross sections in lepton-hadron and e^+e^- hadronic interactions with the help of the dispersion relation techniques. The size of the hadronic corrections strongly depends on the mass of the lepton under study becoming more and more relevant as the lepton mass increases.

The experimental technique to measure a_l: a_e, a_μ, a_τ, is different for the three charged leptons. An extreme precision of 0.28 ppb for a_e is obtained by a single-electron quantum cyclotron frequency measurements [2]. A recent improved observation of the fine structure constant α led to a difference between the measured and predicted a_e negative and significant at 2.4σ's [2].

For the muon, a_μ is measured by comparing the cyclotron and the muon magnetic moment precession frequencies. The recent experiment at Fermilab, "Muon $g-2$," measured a_μ with a precision of 0.46 ppm [3]. The difference between the SM prediction of a_μ, with hadronic contributions calculated via the dispersion relation method [4], and the combined Muon $g-2$ and E821 at Brookhaven National Laboratory experiments, shows a discrepancy of 4.2σ's. However, a new estimate of the theoretical predicted value of a_μ, obtained by recalculating the hadronic contributions using a lattice QCD approach, resulted in a theoretical prediction compatible with the experimental value within 1.2σ's [5].

The theoretical prediction of a_τ, although not as precise as those for lighter leptons, is by far more accurate than the experimental measurements. Theoretically, the larger τ mass makes the hadronic contributions much larger than the case of the electron and the muon and, consequently, also the uncertainties of the a_τ is much larger. Possible contributions to $a_{l,q}$ given from new particles of mass M to the photon-lepton vertex are expected to be on the order of m_l^2/M^2 for a lepton of mass m_l. Therefore, new physics effects for the τ would be enhanced by a factor $m_\tau^2/m_\mu^2 = 286$ with respect to μ. Moreover, in some models addressing recent anomalies in $R_{D^{(*)}}$ [6], a significant contribution to a_τ could arise from new scalar and tensor operators and Δa_τ could be as large as 10^{-3} [7].

The a_τ would also be sensitive to possible lepton compositeness that, in general, would contribute with corrections $O(m_\tau^2/\Lambda_c^2)$, where Λ_c is the "compositeness" scale [8], possibly generated by warped extra dimensions [9–13].

The a_τ investigation definitely represents an excellent tool to access new physics beyond the SM (BSM).

Unfortunately, the present experimental knowledge of a_τ is poor. In fact, the very short τ lifetime precludes the use of the precession frequency measurement method as done in the μ case. The method adopted is to exploit the sensitivity to a_τ of the τ-pair total and differential cross sections, in photon-photon scattering [14]. The best a_τ measurement at LEP was obtained by the DELPHI experiment [16] and provided the limit $-0.052 < a_\tau^{\exp} < 0.013$ at 95% confidence level (CL). The combined reanalysis of various experimental measurements such as the $e^+e^- \to \tau^+\tau^-$ cross section, the transverse τ^- polarization and asymmetry, as well as the decay width $\Gamma(W \to \tau^+\nu_\tau)$, allowed the authors in [17] to set a stronger, but indirect, model-independent limit on new physics contributions to a_τ: $-0.007 < a_\tau < 0.005$. Other strategies to measure the τ anomalous moment at the LHC have been proposed in [18], by considering the rare Higgs decay $h \to \tau\tau\gamma$, which shows a sensitivity at the percent level and the measurement of the distribution of the large transverse mass of τ pairs produced in proton-proton collisions [19].

Recent papers proposed to use ultraperipheral collisions of heavy ions at the LHC to measure the exclusive τ-pair production cross section [20,21]. Using Pb-Pb ultraperipheral collisions (UPC) to single out $\gamma-\gamma$ collisions yielding a τ pair offers several advantages compared with proton-proton collisions at the LHC. In fact, in Pb-Pb collisions, the cross section for $\gamma\gamma \to \tau\tau$ (see Fig. 1) is enhanced by a factor Z^4, largely compensating the lower integrated luminosity compared with that available in proton-proton collisions. In addition, the request of an exclusive final state containing only τ decay products, with essentially no pileup background, allows a better control of the background processes than in case of p-p collisions.

At the LHC, the a_τ measurements have been obtained with Pb-Pb collisions by the ATLAS and CMS experiments. CMS, with an integrated luminosity of 404.3 μb^{-1}, obtained the limit of $-0.088 < a_\tau < 0.056$ at 68% CL [22]. ATLAS, using an integrated luminosity of 1.44 nb^{-1}, provided a limit of $-0.057 < a_\tau < 0.024$ at 95% CL [23]. These measurements at the LHC have still an uncertainty of

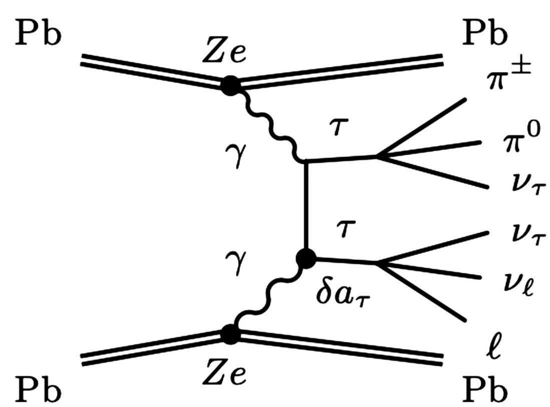

FIG. 1. Pair production of τ leptons from ultraperipheral lead ion (Pb) collisions in two decay modes: hadronic and leptonic. New physics can affect the τ-photon couplings modifying the magnetic moment by δa_τ.

several percents dominated by the statistical error. This uncertainty is expected to be reduced by about 1 order of magnitude with the new data to be collected at High-Luminosity-LHC with an increased integrated luminosity of a factor 10.

A measurement of a_τ is proposed to be performed also at the new τ factories, such as the e^+e^- collider Belle II [24]. It has been estimated that with 50 ab^{-1} the Belle II experiment could set the limit $|a_\tau| < 1.75 \times 10^{-5}$ (1.5% of the SM prediction). Still, at Belle II with an integrated luminosity of 40 fb^{-1} and using polarized electron beams, a precision on a_τ of 10^{-6} could be achieved [25]. However, no systematic uncertainty was taken into account, and the detector response was described by a fast simulation.

The theoretical prediction is $a_\tau^{\mathrm{theo}} = 117721(5) \times 10^{-8}$ [26], where the largest contribution to the uncertainty is due to hadronic effects. By comparing the present a_τ^{exp} with a_τ^{theo} it is clear that the sensitivity of the existing measurements is still more than 1 order of magnitude worse than needed.

The discrepancies between experiment and theory already observed for both a_e and a_μ make the exploration of the τ lepton magnetic moment even more crucial for fundamental physics and more efforts should be devoted especially in refining the experimental methods to measure it.

The growing interest around the rich physics program provided by photon interactions generated by heavy ions at the LHC has also fostered the development of tools to improve the generation of these types of events. It is important to identify tools for event generation that provide a good compromise between flexibility and precision. For this reason, in this work the τ-pair signal production is generated with an effective description in a universal FeynRules output (UFO) model [27] implemented in the Monte Carlo generator MadGraph5 [28]. This choice provides several advantages compared with previous approaches [21], allowing one to distinguish the linear interference between SM and BSM and the pure quadratic BSM contribution. Moreover, an easier and more effective interface among the particle level simulation, the showering/hadronization, and the detector effects is possible. Details on the adopted model will be given in the next section. The detector performance and the experimental environment at the LHC are those of the ATLAS experiment.

In this work, the analysis of data to extract a_τ is performed by exploiting a gradient boosted decision tree (BDTG) [29] approach that optimizes the signal selection together with the best background rejection. To verify the performance of this new approach, the results achieved with the BDTG analysis are compared with those obtained with a standard cut mimicking the one applied in previous LHC experiments. Results refer to an integrated luminosity of 2.0 nb^{-1} corresponding to the total integrated luminosity of the 2015–2018 heavy ion data taking. In addition, results for 1.44 nb^{-1} of integrated luminosity are also quoted to have a direct comparison with the latest published ATLAS results [23].

II. GENERATION OF SIGNAL AND BACKGROUND PROCESSES

In this section, the steps to generate and simulate signal and background processes are discussed. The photon flux implementation and the advantage of using Pb-Pb with respect to proton-proton collisions are discussed in Sec. II A. The signal process $Pb(\gamma) - Pb(\gamma) \to \tau^+\tau^-$ generation, including the contribution from BSM effects, is described in Sec. II B. In this section is also discussed the effect on differential and total cross sections due to a modified value of a_τ. The background processes relevant to this study are presented in Sec. II C. Detector effects have been simulated with a fast simulation as described in Sec. II D.

A. The photon flux

In this work the process $Pb(\gamma) - Pb(\gamma) \to \tau^+\tau^-$ is generated by modifying MadGraph5 to include the photon flux from the lead beams in ultraperipheral collisions following the prescription in Ref. [30]. In the equivalent photon approximation (EPA) [31,32], and neglecting nonfactorizable hadronic interactions between nuclei and nuclear overlap effects, the $\gamma\gamma \to \tau^+\tau^-$ cross section in ultraperipheral Pb-Pb collisions can be expressed as the convolution

$$\sigma^{(\text{Pb-Pb})}(\gamma\gamma \to \tau^+\tau^-) = \int dx_1 dx_2 N(x_1) N(x_2) \hat{\sigma}(\gamma\gamma \to \tau^+\tau^-),$$

where $\hat{\sigma}(\gamma\gamma \to \tau^+\tau^-)$ is the elementary cross section and $N(x_i)$ represents the photon flux from the two Pb ions, calculated as a function of the ratio of the emitted photon energy from the ion i with the beam energy ($x_i = E_i/E_{\mathrm{beam}}$). $N(x_i)$ is described by the classical analytic form [33]

$$N(x_i) = \frac{2Z^2\alpha}{x_i\pi}\left\{\bar{x}_i K_0(\bar{x}_i) K_1(\bar{x}_i) - \frac{\bar{x}_i^2}{2}[K_1^2(\bar{x}_i) - K_0^2(\bar{x}_i)]\right\}$$
$$x_i = E_i/E_{\mathrm{beam}}, \qquad \bar{x}_i = x_i m_N b_{\min}/2, \tag{1}$$

where, for Pb, $Z = 82$, $A = 208$, the nucleon mass $m_N = 0.9315$ GeV, the nucleus radius $R_A \simeq 6.09 A^{1/3}\ \mathrm{GeV}^{-1} \simeq 7$ fm, $b_{\min} \simeq 2R_A$ is the minimum impact parameter, and $K_0(K_1)$ are the modified Bessel functions of the second kind of the first (second) order. The same implementation of the photon flux is also used in [20], where it is found that a more complete treatment of nuclear effects, as included in programs such as SuperChic [34], do not impact significantly

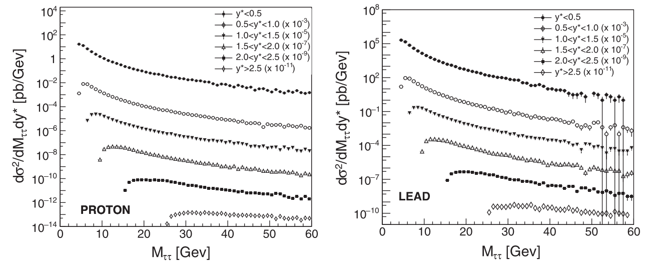

FIG. 2. Double-differential di-τ cross sections as a function of the di-τ mass in bins of half the rapidity separation, y^* ($y^* = |y_1 - y_2|/2$) of the two τ's. The cross sections for proton (left) and lead (right) photon flux are shown.

the cross sections and distributions of the processes that are relevant for our study.

A comparison between the di-τ double-differential cross sections in collisions at the LHC, for proton-proton at $\sqrt{s} = 13$ TeV, and for lead-lead at the nucleon-nucleon energy $\sqrt{s_{NN}} = 5.52$ TeV, is shown in Fig. 2. The proton distributions are obtained using MadGraph5 default configuration, which adopts the EPA improved Weizsacker-Williams formula [35]. The figures show the double-differential di-τ cross sections as a function of the di-τ mass in bins of half the rapidity separation, y^* ($y^* = \frac{|y_1 - y_2|}{2}$), of the two τ's.

The comparison between lead and proton cross sections and their ratio as a function of di-τ mass and of the di-τ rapidity integrated on the di-τ separation and di-τ mass, respectively, are shown in Fig. 3. It is interesting to note that the expected Z^4 enhancement in favor of the radiation intensity from Pb reduces as di-τ mass or rapidity separation increases. In fact, as the di-τ mass (or the di-τ separation) increases, also the Q^2 of the interaction increases, and the interaction radius decreases accordingly. In this situation, the electromagnetic form factor generated by the lead nucleus decreases its effectiveness in photon emission. This effect is encoded in the photon flux dependence on $\bar{x}$ of the analytic form in Eq. (1), which is based on classical electrodynamics.

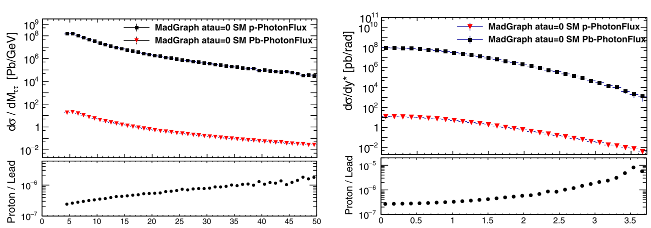

FIG. 3. Differential di-τ cross sections as a function of the di-τ mass (left) and as a function of rapidity separation, y^* ($y^* = |y_1 - y_2|/2$) of the two τ's (right) depending on the photon flux. The ratio of the cross section proton over lead is reported at the bottom of each plot.

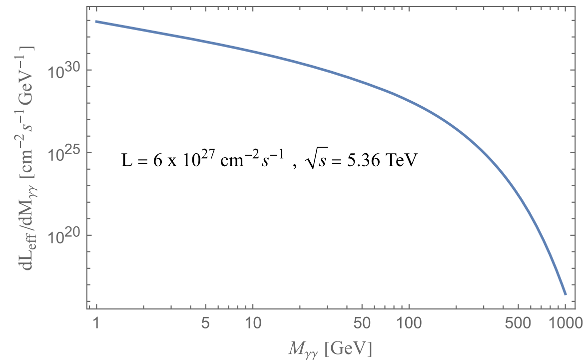

FIG. 4. Effective $\gamma\gamma$ luminosity vs photon-fusion mass in ultraperipheral Pb-Pb collision at $\sqrt{s_{NN}} = 5.36$ TeV.

The cross section in Eq. (1) can be also expressed in terms of an effective $\gamma\gamma$ luminosity ($\frac{dL_{\mathrm{eff}}}{dM_{\gamma\gamma}}$) as

$$\sigma^{(\text{Pb-Pb})}(\gamma\gamma \to \tau^+\tau^-) = \int dM_{\gamma\gamma} \frac{dL_{\mathrm{eff}}}{dM_{\gamma\gamma}} \hat{\sigma}(\gamma\gamma \to \tau^+\tau^-). \quad (2)$$

Figure 4 shows the effective $\gamma\gamma$ luminosity as a function of the photon-fusion mass $M_{\gamma\gamma}$, as obtained from the convolution of the photon flux in Sec. II A.

B. Generation and simulation of the signal

Events including BSM physics through a modified value of a_τ are generated implementing in a UFO model [36], to be used in MadGraph5, the effective Lagrangian term

$$\mathcal{L}_{a_\tau} = a_\tau \frac{e}{4m_\tau} \bar{\tau}_L \sigma^{\mu\nu} \tau_R F_{\mu\nu}, \quad (3)$$

by means of FeynRules [37]. The implementation is validated against theoretical analytical predictions and previous results from LEP [16].

The approach to generate BSM effects here described differs from previous analysis. In fact, the authors in [21] use a custom code, which generates the signal by means of the full form of the photon-τ vertex function and of the cross sections calculated at leading order. The MadGraph5 approach, implementing the signal generation via an effective description in a UFO model, allows an easier interface with showering/hadronization effects and with the detector simulation. Moreover, it also allows one to easily single out the linear interference terms with the SM from the purely BSM quadratic terms. The SM and BSM $\gamma\gamma \to \tau^+\tau^-$ inclusive cross sections here obtained show an agreement within 10% with those in [21].

The study in [20] adopts our same implementation of the photon flux in MadGraph5, as also MadGraph5 for signal simulations. However, [20] makes use of a different UFO model, the SMEFTsim package [38], and extracts the BSM modification to a_τ from the parameters of the SM effective field theory considered in this SMEFTsim code.

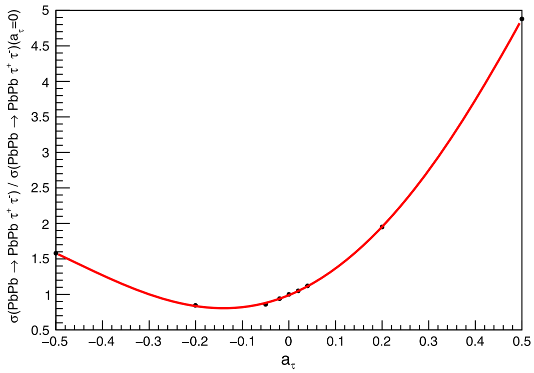

FIG. 5. Ratio between the total ultraperipheral cross sections for $Pb(\gamma) - Pb(\gamma) \to \tau^+\tau^-$ production at the LHC energy $\sqrt{s_{NN}} = 5.02$ TeV and the SM cross section ($a_\tau = 0$) as a function of a_τ. At generation level, a cut on lepton $p_T >$ 1 GeV is applied.

A significant discrepancy is observed between the BSM signal cross section values of [20] and the calculation here presented; on the contrary, the two SM results are in agreement. Since the two BSM calculations rely on an EFT approach, the source of the disagreement is most probably not connected to the EFT but to an issue that occurred in [20] with the conversion between SMEFTsim operators and those generating modification to a_τ. A similar discrepancy is observed between the results in [20] and the BSM cross section calculations reported in [21].

The ratio between the $Pb(\gamma) - Pb(\gamma) \to \tau^+\tau^-$ total cross section and the SM cross section as a function of a_τ is shown in Fig. 5, where the ratio is set to 1 for $a_\tau = 0$, considered as the SM value. The asymmetry between positive and negative a_τ values is due to interference between the SM part and the BSM modified τ coupling. The effect of different a_τ values is investigated by looking at various τ and di-τ kinematical distributions. In particular, Fig. 6 shows the leading τ p_T, the leading τ rapidity, the di-τ system rapidity, and invariant mass distributions for three representative values of a_τ $(0, \pm 0.4)$ normalized to 2 nb^{-1} of integrated luminosity. Figure 6 proves that, in addition to the τ-pair cross section, also the differential cross sections, and especially the τp_T distribution, can be exploited to improve the sensitivity to a_τ.

The τ decays, the hadronization, and the shower processes are described with PYTHIA8 [39]. For each signal sample, 2×10^6 events have been generated, varying the coupling a_τ from -0.04 to $+0.04$ (see Appendix A for the complete list and statistics). see Appendix A and Table VII for the complete list and statistics.

C. Background processes

The requirement of selecting exclusive di-τ decay products in UPC events greatly reduces the background contribution in the signal selection. The background processes

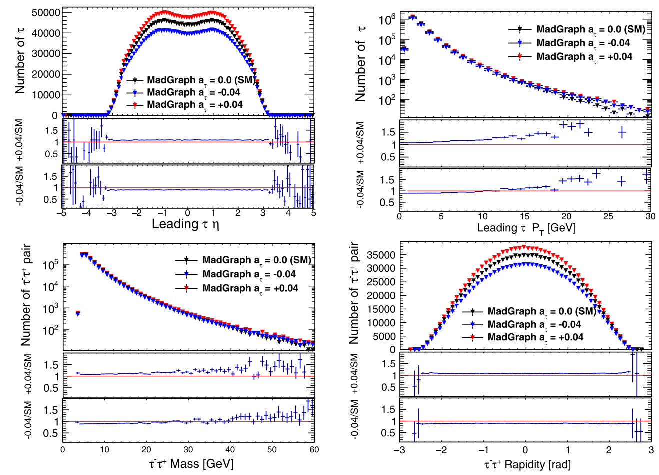

FIG. 6. Top: leading $\tau\,\eta$ and p_T distributions for different values of a_τ: $+0.04$, -0.04, 0. The ratio between $a_\tau = \pm 0.04$ and $a_\tau = 0$ is reported on the bottom side of each plot. Bottom: di-τ system mass and rapidity distributions at different values of a_τ: $+0.04$, -0.04, 0. The ratios are reported on the bottom side of the plots.

considered are $\gamma\gamma \to e^+e^-$, $\gamma\gamma \to \mu^+\mu^-$, $\gamma\gamma \to b\bar{b}$, and $\gamma\gamma \to \mathrm{jet}(c, s, u, d)\mathrm{jet}(\bar{c}, \bar{s}, \bar{u}, \bar{d})$. Among these processes, the $\gamma\gamma \to \mu^+\mu^-$ processes where one of the μ radiate a photon is the major source of background. As shown in [20,21], the $\gamma\gamma \to \bar{q}q$ produces a larger charged-particle multiplicity than the signal and hence can be totally rejected by exclusivity requirements.

Other contributions to the background could be due to diffractive photonuclear events, mediated by a Pomeron exchange, where the Pb ions may not dissociate and some particles could be produced in the central rapidity region. For this background, a reliable Monte Carlo simulation is not available; however, in Ref. [23] it was estimated by a data-driven method that this contribution results in an about 2% contribution to the $\tau^+\tau^-$ data sample. In this analysis, this contribution has been neglected.

We produced 2×10^6 events of background samples with PYTHIA8, see Appendix A for details.

D. Simulation of detector effects

The simulation of the ATLAS detector is done by using DELPHES 3.5.0 framework [40]. This package implements a fast simulation of the detector, including a track propagation system embedded in a magnetic field, the electromagnetic and hadron calorimeter responses, and a muon identification system. Physics objects such as electrons or muons are then reconstructed from the simulated detector response using dedicated subdetector resolutions. For the analysis here presented, electron [41] and muon [42] efficiencies have been modified using the latest ATLAS performance results as obtained on the data sample collected in 2015–2018 (Table I). Other efficiencies such as the tracking efficiency,

TABLE I. Tracking efficiencies, as applied in DELPHES, for electrons [41] and muons [42] for different $\eta \times p_T$ bins.

Particle	η and p_T (GeV)	Efficiency (ϵ)
Electron	$\lvert\eta\rvert > 2.4$ or $p_T <= 4.5$	0.00
	$\lvert\eta\rvert <= 2.4$ and $4.5 > p_T < 30.0$	0.82
	$\lvert\eta\rvert <= 2.4$ and $30.0 > p_T < 40.0$	0.86
	$\lvert\eta\rvert <= 2.4$ and $40.0 > p_T <= 60.0$	0.88
	$\lvert\eta\rvert <= 2.4$ and $p_T > 60.0$	0.92
Muon	$\lvert\eta\rvert > 2.5$ or $p_T <= 3.5$ GeV	0.00
	$\lvert\eta\rvert <= 2.5$ and $3.5 > p_T < 4.0$	0.65
	$\lvert\eta\rvert <= 2.5$ and $4.0 > p_T < 5.0$	0.80
	$\lvert\eta\rvert <= 2.5$ and $p_T > 5.0$	0.95

the smearing reconstruction, or the energy resolution functions are used without changes [40,43,44].

III. ANALYSIS PROCEDURE

In this section, the procedure to select the signal from the background processes is described. The analysis is applied to the data including the fast detector simulation. The preselection cuts and the signal region definition are described in Sec. III A. The two analysis procedures based on standard cuts (SCs) and on a multivariate approach (BDTG), respectively, are presented in Sec. III B.

A. Preselection and signal region definition

Event selection requires at least one τ decayed leptonically. The second τ is requested to decay hadronically and is reconstructed requiring one or three tracks. Two signal regions are identified according to the τ decay topologies: one lepton, one track (1L1T) and one lepton, three tracks (1L3T), respectively. These requirements potentially collect about 22% of all possible τ-pair decays, as shown in Table II. The signal region where both the τ's decay leptonically is not included in this analysis due to the low statistics obtained after the lepton identification, see Table XI in Appendix C for more details. The final state with leptons is fundamental for the trigger selection.

Preselection cuts, mimicking the minimal ATLAS object selection, are applied on leptons: $p_T > 4.5(3.5)$ GeV and $|\eta| < 2.4(2.5)$ for electrons (muons). In addition, each track is requested to satisfy minimal acceptance criteria: $p_T^{(\mathrm{track})} > 500$ MeV and $|\eta^{(\mathrm{track})}| < 2.5$. The preselection cuts are summarized in Table III. The lepton and track multiplicities for signal and background processes after the preselection cuts are shown in Fig. 7; the plots show that a requirement of a single lepton and one or three tracks collect most of the signal events, rejecting a large fraction of the background.

TABLE II. τ decay branching fractions.

τ decay definition	τ decay process	Branching fraction (%)
Lepton decay	$\tau^- \to e^- \bar{\nu}_e \nu_\tau$	17.85
	$\tau^- \to \mu^- \bar{\nu}_\mu \nu_\tau$	17.36
One charged pion decay	$\tau^- \to \pi^- \nu_\tau n\pi^0$ $(n = 0, 1, 2, 3)$	46.75
Three charged pion decay	$\tau^- \to 2\pi^- \pi^+ \nu_\tau n\pi^0$ $(n = 0, 1)$	13.91

TABLE III. Preselection cut summary.

Preselection	Cuts
Electron identification	$p_T > 4.5$ GeV, $\lvert\eta\rvert < 2.4$
Muon identification	$p_T > 3.5$ GeV, $\lvert\eta\rvert < 2.5$
Track identification	$p_T^{(\mathrm{track})} > 500$ MeV, $\lvert\eta^{(\mathrm{track})}\rvert < 2.5$

B. Signal extraction: SC and BDTG selections

The signal and background distributions of kinematic variables of interest after the preselection cuts are shown in Figs. 8 and 9 for 1L1T and 1L3T signal regions, respectively. These distributions include all the background processes described in Sec. II C and are normalized to 2.0 nb^{-1} of integrated luminosity. The acoplanarity variable between the muon and the track (three track system) is defined as acoplanarity $= 1 - |\Delta\phi_{\mu,\mathrm{trk}(s)}|/\pi$, while the missing transverse energy (E_T^{Miss}) is calculated from calorimeter energy deposits $[\vec{p}_T(i)]$ as $E_T^{\mathrm{Miss}} = |\vec{E}_T^{\mathrm{Miss}}| = |\sum_i \vec{p}_T(i)|$. The acoplanarity and the missing transverse energy distributions for SR1L1T show, as expected, a strong difference between signal and background due to the presence of neutrinos from τ decays. The number of simulated background events, after the preselection for the 1L3T signal region (SR), is very limited; however, the invariant mass of the three nonlepton track ($\mathrm{Mass}_{3\mathrm{T}}$) plot shows a significant separation between signal and backgrounds. The lepton p_T for both signal regions do not show any significant discrimination between the signal and the background sample. The cut applied on muon p_T is increased to 4 GeV for both the signal regions to apply the same efficiency of the electron identification and to mimic the muon threshold used in the ATLAS trigger.

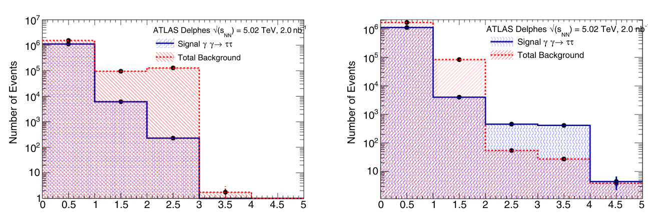

FIG. 7. Lepton (left) and track (right) multiplicities for signal and background processes after the preselection cuts.

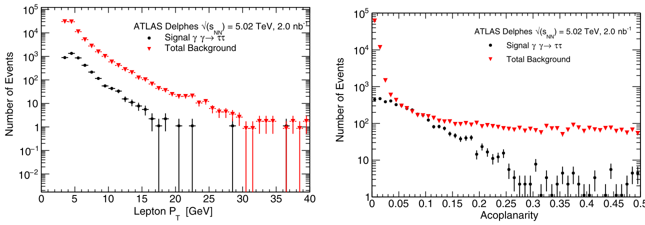

FIG. 8. Distributions of the leading lepton p_T and of the acoplanarity after the preselection for the signal region 1L1T.

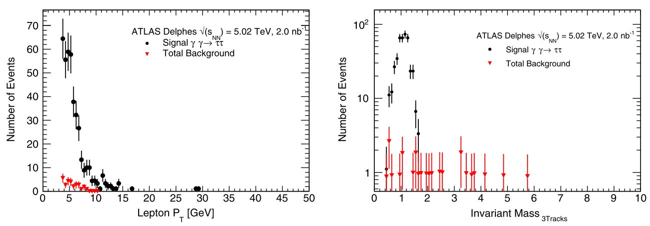

FIG. 9. Distributions of the leading lepton p_T and the invariant mass of the three tracks Mass_{3T} after the preselection for the signal region 1L3T.

The applied kinematic selection for the SC analysis is as follows:

(i) 1L1T: In order to reduce the overlap with the lepton, the track must fulfill an angular requirement: $\Delta\mathrm{R}(\mathrm{lepton}-\mathrm{trk}) > 0.02$ [45]. The total charge of track plus lepton must be zero. In order to reduce the dilepton background, the lepton-track system is required to fulfill the cut: acoplanarity < 0.4.

(ii) 1L3T: The three tracks are required not to overlap the lepton by applying the ΔR cut defined above. The total charge of the three tracks plus the lepton must be zero.

The invariant mass of the three nonlepton tracks (Mass_{3T}) is required to satisfy $\mathrm{Mass}_{3T} < 1.7$ to help the identification of the τ lepton. The acoplanarity < 0.2 requirement is also applied to reduce the lepton background.

A summary of the SC selection for 1L1T and 1L3T is shown in Table IV.

TABLE IV. Selection cuts named as SC dedicated to the identification of the SRs applied to the lepton objects and to the tracks after the preselection cuts.

SR1L1T	SR1L3T
1 lepton	1 lepton
1 track	3 tracks
$\mathrm{Charge}_{1L1T} = 0$	$\mathrm{Charge}_{1L3T} = 0$
	$\mathrm{Mass}_{3T} < 1.7$ GeV
Acoplanarity < 0.4	Acoplanarity < 0.2
$p_T^{\mathrm{Muon}} > 4$ GeV	$p_T^{\mathrm{Muon}} > 4$ GeV

TABLE V. The BDTG ranking of the variables used, divided per SR.

SR1L1T	SR1L3T
$\phi - \mathrm{MissingE_T}$	ΣP_T 3 tracks (3 track system p_T)
Track η	Invariant mass (lepton + 3 tracks)
Lepton ϕ	Lepton P_T
Lepton η	Invariant mass (3 tracks)
Missing E_T	ΔR (lepton, 3 track system)
Acoplanarity	$\Delta\phi$ (lepton, 3 track system)
Track P_T	Missing E_T
Invariant mass (lepton + track)	ΔR (lepton, track)
ΔR (lepton, track)	Track P_T
Lepton P_T	Acoplanarity
$\Delta\phi$ (lepton, track)	$\Delta\phi$ (lepton, track)
H_T $[\sum_i \lvert\vec{p}_T(i)\rvert]$	H_T $[\sum_i \lvert\vec{p}_T(i)\rvert]$

In order to investigate possible improvements in the signal over background ratio, a multivariate analysis has been implemented using a gradient boosted decision tree in the toolkit for multivariate data analysis framework [46]. The BDTG aims at improving the selection by fully exploiting the final state kinematical variables. The complete list of the variables used for the two signal regions, ordered by BDTG ranking, is reported in Table V. The BDTG distributions are shown in Fig. 10 for signal and background processes for the two signal regions. The signal selection is obtained by applying thresholds on the BDTG distributions. The two thresholds, for 1L1T and 1L3T, are obtained based on best significance criterion with significance defined as $\mathrm{S}/\sqrt{\mathrm{S}+\mathrm{B}}$.

For 1L1T, the BDTG threshold is set to $\mathrm{BDTG} > 0.84$ corresponding to a significance of 58 to be compared with a significance of 27 obtained with the SC analysis at 2 nb^{-1} of integrated luminosity. For the signal region 1L3T, the cut on BDTG is set to $\mathrm{BDTG} > -0.61$ with a significance of 20 to be compared with a significance of 18 obtained with the SC analysis at 2 nb^{-1} of integrated luminosity.

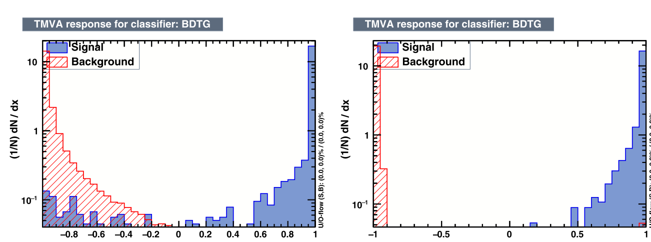

FIG. 10. BDTG distributions for signal and background processes for the 1L1T (left) and 1L3T (right) signal regions.

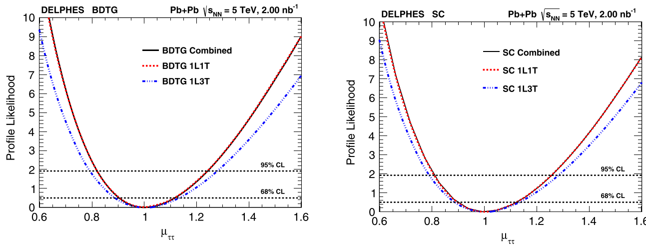

FIG. 11. Profile likelihood scan of the signal strength parameter using Asimov data and considering $a_\tau = 0$ for the two signal regions. Left: results for the BDTG selection. Right: results for the SC. The normalization systematic uncertainties included are 2% to mimic the ATLAS luminosity uncertainties and an additional uncorrelated 10% for signal and background to overall mimic experimental conditions. The integrated luminosity is set to 2.0 nb^{-1}.

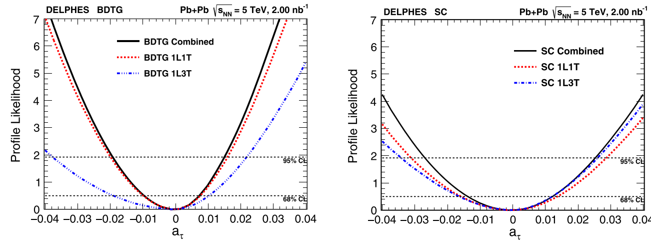

FIG. 13. Profile likelihood for a_τ using Asimov data for the two signal regions and the combination of the two regions. Left: results for the BDTG selection. Right: results for the SC. The normalization systematic uncertainties included are 2% to mimic the ATLAS luminosity uncertainties and an additional uncorrelated 10% for signal and background to overall mimic experimental conditions. The integrated luminosity is set to 2.0 nb^{-1}.

IV. SENSITIVITY TO THE τ ANOMALOUS MAGNETIC MOMENT

In this section, the sensitivity to the signal strength $\mu_{\tau\tau}$, defined as the ratio of the observed signal yield to the SM expectation assuming the SM value for $\mu_{\tau\tau} = 1$, and to the anomalous magnetic moment a_τ are presented. Both estimates, carried out using a profile likelihood fit [47] in the lepton transverse momentum distributions, are obtained for the SC and the BDTG analyses.

The sensitivity to the signal strength $\mu_{\tau\tau}$ in 95% CL is measured to be $\mu_{\tau\tau} = 1^{-0.189}_{+0.256}$ and $\mu_{\tau\tau} = 1^{-0.179}_{+0.241}$ for the SC and BDTG analysis, respectively. These estimates are obtained using Asimov data. The included systematic uncertainties of normalization are the luminosity estimated to be 2% and an additional conservative uncorrelated 10% assigned to signal and background to take into account the experimental conditions. These results are illustrated in the plots of Fig. 11 where a clear improvement of the $\mu_{\tau\tau}$ precision is shown with the BDTG approach. The sensitivity obtained for the two signal regions and for the two analysis selections presented in this work are compared to the ATLAS measurement obtained with sequential cuts in Fig. 12. In this figure, the integrated luminosity of the two analysis selections is scaled to 1.44 nb^{-1}, the same integrated luminosity of the quoted ATLAS results.

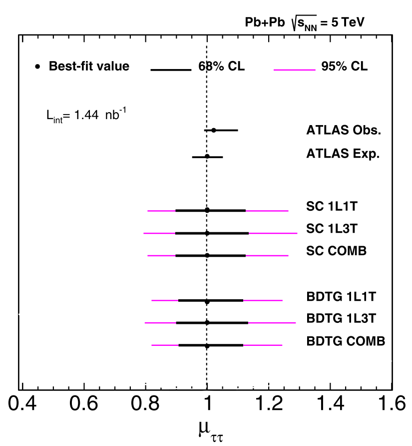

FIG. 12. Sensitivity for $\mu_{\tau\tau}$ signal strength using Asimov data for the two signal regions and for the combination using BDTG and SC selections using 1.44 nb^{-1} of integrated luminosity. The normalization systematic uncertainties included are the ATLAS luminosity estimated as 2% and an additional uncorrelated 10% to signal and background to overall mimic experimental conditions. These results are compared with existing results from ATLAS (expected and observed) obtained by using 1.44 nb^{-1} of integrated luminosity [23]. A point denotes the best-fit value for each measurement where available, while thick black (thin magenta) lines show 68% CL (95% CL) intervals.

The sensitivity to a_τ is estimated with a fit where a_τ is the only free parameter and using the lepton transverse momentum distribution with a nominal value of a_τ set to the SM value ($a_\tau = 0$). Simulated signal samples with various a_τ values are included in the fit. The profile likelihood scans are presented in Fig. 13. The sensitivity to a_τ at 95% CL are $a_\tau = 0^{-0.19}_{+0.15}$ and $a_\tau = 0^{-0.027}_{+0.025}$ using the BDTG and SC analysis, respectively. A clear improvement in the sensitivity to a_τ is shown when using the BDTG approach. All the results are shown in the Table VI.

The sensitivity obtained on a_τ with the BDTG analysis is compared with previous measurements in Fig. 14. The

TABLE VI. The sensitivity to $\mu_{\tau\tau}$ and a_τ at 95% CL for each signal region and the combination of the two. The two methods, BDTG and SC, are compared. The integrated luminosity is set to 2.0 nb^{-1}.

95% CL	SR1L1T	SR1L3T	Combined
SC	$\mu_{\tau\tau} = 1^{-0.189}_{+0.257}$	$\mu_{\tau\tau} = 1^{-0.198}_{+0.282}$	$\mu_{\tau\tau} = 1^{-0.189}_{+0.256}$
BDTG	$\mu_{\tau\tau} = 1^{-0.179}_{+0.242}$	$\mu_{\tau\tau} = 1^{-0.195}_{+0.277}$	$\mu_{\tau\tau} = 1^{-0.179}_{+0.241}$
SC	$a_\tau = 0^{-0.031}_{+0.030}$	$a_\tau = 0^{-0.034}_{+0.026}$	$a_\tau = 0^{-0.027}_{+0.025}$
BDTG	$a_\tau = 0^{-0.020}_{+0.016}$	$a_\tau = 0^{-0.038}_{+0.022}$	$a_\tau = 0^{-0.019}_{+0.015}$

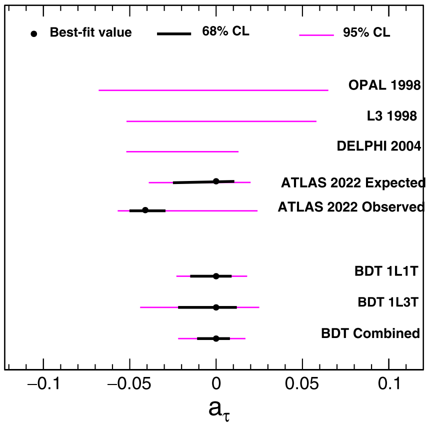

FIG. 14. Best-fit value of a_τ parameter using Asimov data for the two signal regions and the combination using the BDTG selection with an integrated luminosity of 1.44 nb^{-1}. The systematic uncertainties included are the ATLAS luminosity estimated as 2% and an additional 10% to overall mimic experimental conditions. These results are compared with existing results from OPAL [48], L3 [49], DELPHI [16], and the latest results from ATLAS obtained with an integrated luminosity of 1.44 nb^{-1} (expected and observed limits). A point denotes the best-fit value for each measurement where available, while thick black (thin magenta) lines show 68% CL (95% CL) intervals.

integrated luminosity of the BDTG analysis in this figure is scaled to 1.44 nb^{-1}, the same integrated luminosity of the latest ATLAS results.

V. CONCLUSIONS

A study was presented of the ultraperipheral process $Pb(\gamma) - Pb(\gamma) \to \tau^+\tau^-$ using a signal and background simulation, based on experimental conditions and detector performances of the ATLAS experiment at the CERN LHC. One τ is required to decay leptonically while the other one decays hadronically, into one or three tracks. This study aims at an estimation of the precision in the signal strength $\mu_{\tau\tau}$ measurement and of the sensitivity achievable in the determination of the τ anomalous magnetic moment a_τ.

A different approach than in previous studies was adopted by using the signal events produced by an effective a_τ-generating Lagrangian term, implemented in the MadGraph5 Monte Carlo generator. Signal and background events were normalized at a luminosity of 2.0 nb^{-1}. The signal selection was performed with a SC procedure and with a new BDTG approach.

As a result,

(i) the signal strength $\mu_{\tau\tau} 1^{-0.179}_{+0.241}$ at 95% CL was achieved with the BDTG selection, to be compared with $\mu_{\tau\tau} = 1^{-0.189}_{+0.256}$ obtained with the SC procedure;

(ii) the sensitivity to a_τ at 95% CL resulted to be $a_\tau = 0^{-0.019}_{+0.015}$ by using the BDTG method and $a_\tau = 0^{-0.027}_{+0.025}$ by using the SC selection.

Our results show that, using the BDTG approach, a significant improvement in precision could be obtained for both $\mu_{\tau\tau}$ and a_τ determinations compared to the sequential cuts procedure used by the ATLAS experiment [23]. The present expected ATLAS sensitivity to a_τ is about 0.06 (at 95% CL) dominated by statistics (0.045).

In this work, we introduced a systematic uncertainty of 2% from LHC luminosity and an additional conservative uncorrelated 10% assigned to the overall $\gamma\gamma \to \mu\mu$ production cross section yielding a sensitivity to a_τ of 0.034 and 0.052 for the BDT approach and the cut-flow procedure, respectively, with an improvement of $\approx$35% in favor of BDT.

However, these results look still insufficient to explore new physics. It would be desirable to obtain at least a sensitivity of $\approx 10^{-3}$ in a_τ measurement, so approaching the order of magnitude expected in the SM, dominated by one loop contribution in QED.

In fact, it is worth noting that there are new physics models predicting a_τ as large as $\approx 10^{-3}$ [7].

We believe that with the upcoming experiments in proton-proton and heavy ions collisions at the LHC and e^+e^- collisions at Belle II, thanks to higher collected luminosities, but also with the help of new analysis procedures, the a_τ measurements could be performed with a precision better by at least 1 order of magnitude than done in the past, providing a new window in the search for new physics.

ACKNOWLEDGMENTS

We thank the $g-2$ tau ATLAS working group, in particular, M. Dyndal and L. Beresford, for the useful discussion on the expected a_τ results and private communications. We thank P. Paradisi and A. Strumia for useful discussions. N. V. thanks G. Landini, A. Strumia, and J. Wang for help in the validation of the UFO model. The work of N. V. was partially supported by ICSC—Centro Nazionale di Ricerca in High Performance Computing, Big Data, and Quantum Computing, funded by European Union—NextGenerationEU, reference code CN_00000013.

APPENDIX A: MONTE CARLO DISTRIBUTIONS AND CROSS SECTIONS

Several background samples have been included in this analysis; 2×10^6 events for each sample have been generated and simulated. Table VII reports the complete list of the samples used with the production cross section

TABLE VII. Total cross sections of each sample included in the analysis. A cut on $p_T > 1$ GeV and $\eta < 2.5$ of the lepton is applied at generation level. Different signal samples have been produced depending on the anomalous magnetic coupling value.

Sample	Cross section (pb)	Events at 2 nb^{-1}
SM $(a_\tau = 0)$	$5.49 \times 10^8 \pm 1.7 \times 10^5$	1.111111×10^6
SM + BSM $(a_\tau = +0.02)$	$5.79 \times 10^8 \pm 1.9 \times 10^5$	1.176470×10^6
SM + BSM $(a_\tau = -0.02)$	$5.22 \times 10^8 \pm 1.8 \times 10^5$	1.052631×10^6
SM + BSM $(a_\tau = -0.01)$	$5.35 \times 10^8 \pm 1.7 \times 10^5$	1.081081×10^6
SM + BSM $(a_\tau = +0.01)$	$5.64 \times 10^8 \pm 1.8 \times 10^5$	1.142857×10^6
SM + BSM $(a_\tau = -0.04)$	$4.99 \times 10^8 \pm 1.6 \times 10^5$	998000
SM + BSM $(a_\tau = +0.04)$	$6.12 \times 10^8 \pm 1.9 \times 10^5$	1.212121×10^6
$\gamma\gamma \to e^- e^+$	$4.258 \times 10^8 \pm 1.8 \times 10^8$	869565
$\gamma\gamma \to \mu^- \mu^+$	$4.258 \times 10^8 \pm 1.8 \times 10^8$	869565
$\gamma\gamma \to bb$	$1.629 \times 10^6 \pm 2,3 \times 10^2$	3257
$\gamma\gamma \to cc$	$3.276 \times 10^6 \pm 1.3 \times 10^5$	6557
$\gamma\gamma \to \mathrm{jet}(c,d,u)\mathrm{jet}(c,d,u)$	$3.686 \times 10^6 \pm 1.5 \times 10^5$	7380

and the expected number of events at 2.0 nb^{-1} of integrated luminosity. Cuts on lepton $p_T > 1$ GeV and $\eta < 2.5$ are applied at generation level.

Figure 15 shows the distributions of τ and di-τ system for the value of $a_\tau = \pm 0.02$ compared with the nominal Standard Model $a_\tau = 0$.

APPENDIX B: BOOSTED DECISION TREE

In this appendix, the BDTG observables used in the evaluation are shown for each channel. The background sample used is the sum of the background channels already shown in Table VII.

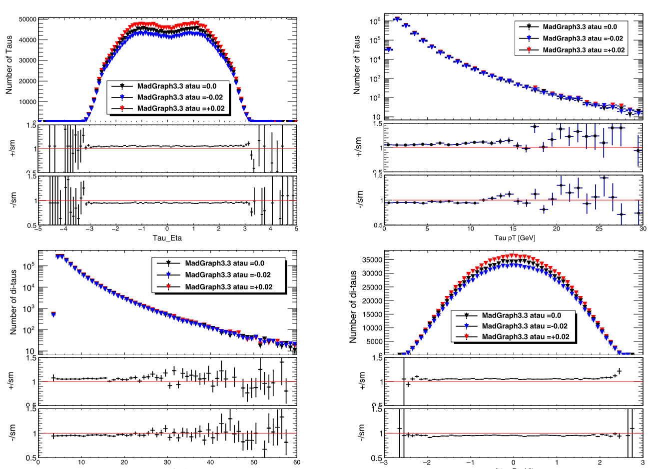

FIG. 15. Top: $\tau\,\eta$ and p_T distributions at different values of a_τ: $+0.02$, -0.02, 0. The ratio between $a_\tau = \pm 0.02$ and $a_\tau = 0$ is reported on the bottom side of each plots. Bottom: di-τ system mass and rapidity distributions at different values of a_τ: $+0.02$, -0.02, 0. The ratios are reported on the bottom side of the plots.

Figures 16 and 17 report for 1L3T and 1L1T, respectively, the distributions of the variables used for the selection.

APPENDIX C: PROFILE LIKELIHOOD AT 1.44 nb^{-1} INTEGRATED LUMINOSITY

In this appendix, the profile likelihoods obtained for 1.44 nb^{-1} integrated luminosity are shown. This integrated luminosity corresponds to the integrated luminosity

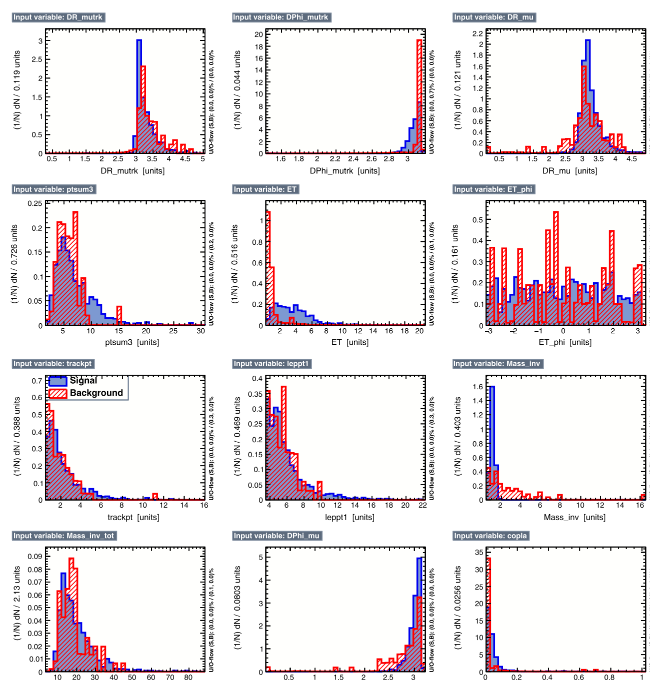

FIG. 16. Distributions of the observable used for the SR1L3T BDT analysis.

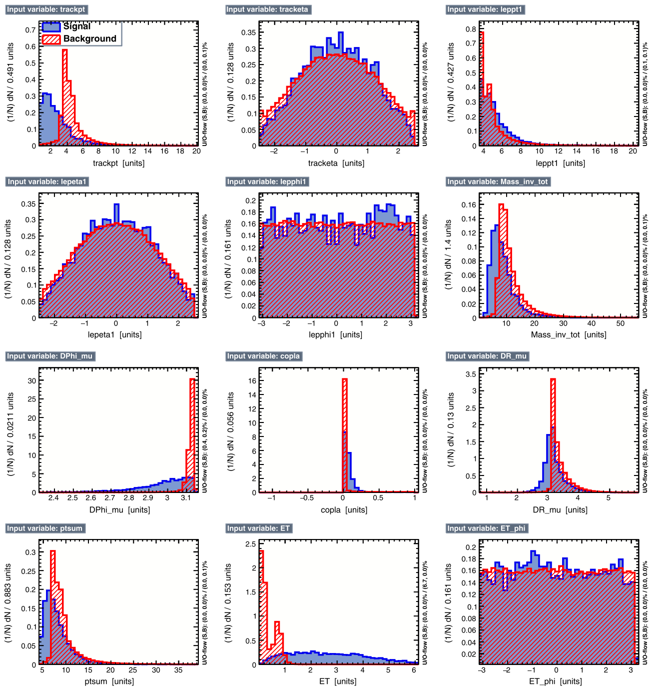

FIG. 17. Observables used for the SR1L1T BDT analysis.

collected with heavy ion collisions in the year 2018 (2015 excluded).

The sensitivity to the signal strength $\mu_{\tau\tau}$ at 95% CL are measured to be $\mu_{\tau\tau} = 1^{-0.194}_{+0.264}$ and $\mu_{\tau\tau} = 1^{-0.181}_{+0.244}$ for the SC and BDTG analysis, respectively. These estimates are obtained using Asimov data. The normalization systematic uncertainties included are the luminosity estimated to be 2% and an additional uncorrelated 10% assigned to signal and to background to take into account the experimental conditions. These results are illustrated in the plots of Fig. 18 where a clear improvement of the $\mu_{\tau\tau}$ precision is shown with the BDTG approach.

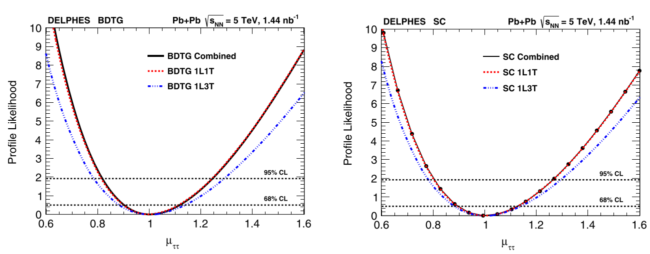

FIG. 18. Profile likelihood scan of the signal strength parameter using Asimov data and considering $a_\tau = 0$ for the two signal regions. Left: results for the BDTG selection. Right: results for the SC. The systematic uncertainties included are on the luminosity, estimated to be 1.44% and an additional uncorrelated 10% to signal and background to conservatively mimic the experimental conditions.

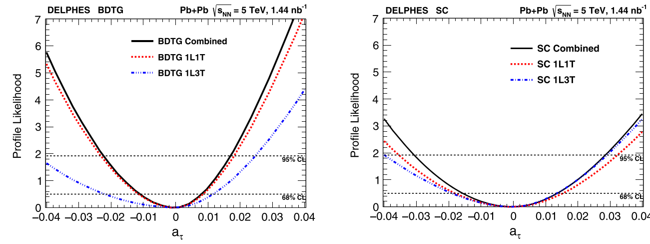

FIG. 19. Profile likelihood for a_τ using Asimov data for the two signal regions and the combination of the two regions. Left: results for the BDTG selection. Right: results for the SC. The systematic uncertainties included are 2% to mimic the ATLAS luminosity uncertainties and an additional uncorrelated 10% to signal and background to overall mimic experimental conditions.

The sensitivity to a_τ is estimated with a fit where a_τ is the only free parameter and using the lepton transverse momentum distribution with a nominal value of a_τ set to the SM value ($a_\tau = 0$). Simulated signal samples with various a_τ values are included in the fit. The profile likelihood scans are presented in Fig. 19. The sensitivity to a_τ at 95% CL are $a_\tau = 0^{-0.022}_{+0.017}$ and $a_\tau = 0^{-0.031}_{+0.029}$ using the BDTG and SC analysis, respectively. A clear improvement in the sensitivity to a_τ is shown when using the BDTG approach (Table VIII)

APPENDIX D: SELECTION CUT FLOW

In this appendix, the selection cuts applied to all the signal regions are shown. The dilepton signal region is also included for completeness; however, the low statistics preclude the test of the BDT method. Therefore, the two lepton signal region (2LSR) is also removed from the final limits comparison. Tables IX, X and XI report the event yields after each cut normalized to 2 nb^{-1} of integrated luminosity for the SR1L1T, SR1L3T, and 2LSR.

TABLE VIII. The sensitivity to $\mu_{\tau\tau}$ and a_τ at 95% CL for each signal region and the combination of the two. The two methods, BDTG and SC, are compared.

95% CL	SR1L1T	SR1L3T	Combined
SC	$\mu_{\tau\tau} = 1^{-0.195}_{+0.265}$	$\mu_{\tau\tau} = 1^{-0.207}_{+0.293}$	$\mu_{\tau\tau} = 1^{-0.194}_{+0.264}$
BDTG	$\mu_{\tau\tau} = 1^{-0.181}_{+0.245}$	$\mu_{\tau\tau} = 1^{-0.204}_{+0.288}$	$\mu_{\tau\tau} = 1^{-0.181}_{+0.244}$
SC	$a_\tau = 0^{-0.035}_{+0.032}$	$a_\tau = 0^{-0.040}_{+0.029}$	$a_\tau = 0^{-0.031}_{+0.029}$
BDTG	$a_\tau = 0^{-0.023}_{+0.018}$	$a_\tau = 0^{-0.044}_{+0.025}$	$a_\tau = 0^{-0.022}_{+0.017}$

TABLE IX. Event yield after each cut at 2 nb^{-1} for each a_τ value generated.

Selection Cuts	a_τ −0.04	a_τ −0.02	a_τ −0.01	a_τ SM 0	a_τ +0.01	a_τ +0.02	a_τ +0.04
Total event	1×10^6	1.052631×10^6	1.081081×10^6	1.111111×10^6	1.142857×10^6	1.176470×10^6	1.212121×10^6
SR1L1T							
1 lepton	5828.5	5804.41	5766.66	6075.59	6113.13	6580.31	7057.2
1 track	3917	3905.02	3923.1	4031.52	4091.79	4422.94	4804.2
$\mathrm{Charge}_{1\mathrm{L}1\mathrm{T}} = 0$	3853	3845.06	3864.24	3967.14	4030.69	4349.44	4729.2
Acoplanarity < 0.4	1757.5	1811.02	1773.9	1893.11	1872.31	2029.78	2149.2
$P_T^{\mathrm{Muon}} > 4$ GeV	1320	1336.04	1318.14	1403.04	1374.4	1513.51	1596.6
$E_T^{\mathrm{Miss}} > 1$ GeV	1220.5	1237.15	1213.92	1283.16	1259.63	1392.97	1480.2
SR1L3T							
1 lepton	5828.5	5804.41	5766.66	6075.59	6113.13	6580.31	7057.2
3 tracks	422	410.28	371.52	416.81	433.39	450.99	488.4
$\mathrm{Charge}_{1\mathrm{L}3\mathrm{T}} = 0$	420.5	409.23	369.36	416.25	431.68	450.41	487.2
$\mathrm{Mass}_{3\mathrm{T}} < 1.7$ GeV	420	403.97	365.58	413.48	426.54	449.23	484.8
Acoplanarity < 0.2	403	383.98	345.06	390.72	403.13	420.42	459.6
$P_T^{\mathrm{Muon}} > 4$ GeV	344	327.70	299.7	323.01	336.32	355.74	397.8

TABLE X. Event yield after each cut at 2 nb^{-1} for SR1L1T and SR1L3T.

Selection	$\gamma\gamma \to \tau\tau$	$\gamma\gamma \to \mu\mu$	$\gamma\gamma \to ee$	$\gamma\gamma \to bb$	$\gamma\gamma \to cc$	$\gamma\gamma \to jj$
Total event	1.111111×10^6	869565	869565	3245.91	6557.38	7380.07
SR1L1T						
1 Lepton	6081.06	57964.6	35241.6	18.96	0.31	0.03
1 Track	4035.15	54400.6	27396.2	1.43	0.05	0
$\mathrm{Charge}_{1\mathrm{L}1\mathrm{T}} = 0$	3970.71	54399.7	27395	0.88	0.02	0
Acoplanarity < 0.4	1894.81	1193.53	435.71	0.52	0.003	0
$P_T^{\mathrm{Muon}} > 4$ GeV	1404.3	746.75	435.71	0.31	0.003	0
SR1L3T						
1 lepton	6081.06	57964.6	35241.6	18.96	0.31	0.03
3 tracks	417.18	13.62	5.53	3.82	0.09	0.09
$\mathrm{Charge}_{1\mathrm{L}3\mathrm{T}} = 0$	416.63	13.19	5.53	1.91	0.05	0
$\mathrm{Mass}_{3\mathrm{T}} < 1.7$ GeV	413.85	5.96	2.55	0.40	0.01	0.01
Acoplanarity < 0.2	391.07	5.96	1.70	0.35	0.01	0.01
$P_T^{\mathrm{Muon}} > 4$ GeV	323.30	4.68	1.70	0.23	0.01	0.01

TABLE XI. Event yield after each cut at 2 nb^{-1} for each sample generated (2LSR only).

Selection	$\gamma\gamma \to \tau\tau$	$\gamma\gamma \to \mu\mu$	$\gamma\gamma \to ee$	$\gamma\gamma \to bb$	$\gamma\gamma \to cc$	$\gamma\gamma \to jj$
Total event	1.111111×10^6	869565	869565	3245.91	6557.38	7380.07
2LSR						
1 muon + 1 electron	117.77	0.85	0.85	0.05	0	0
Charge = 0	117.77	0.43	0.85	0.04	0	0
$P_T^{\mathrm{Muon}} > 4.0$ GeV	101.66	0.43	0.85	0.03	0	0
N_{trk} in $\Delta R_{\mathrm{lep-trk}} > 0.1 = 0$	101.66	0.43	0.85	0.03	0	0

[1] J. Schwinger, On quantum-electrodynamics and the magnetic moment of the electron, Phys. Rev. **73**, 416 (1948).

[2] D. Hanneke, S. Fogwell Hoogerheide, and G. Gabrielse, Cavity control of a single-electron quantum cyclotron: Measuring the electron magnetic moment, Phys. Rev. A **83**, 052122 (2011).

[3] B. Abi *et al.* (Muon $g-2$ Collaboration), Measurement of the positive muon anomalous magnetic moment to 0.46 ppm, Phys. Rev. Lett. **126**, 141801 (2021).

[4] T. Aoyama, N. Asmussen, M. Benayoun, J. Bijnens, T. Blum *et al.*, The anomalous magnetic moment of the muon in the standard model, Phys. Rep. **887**, 1 (2020).

[5] Sz. Borsanyi *et al.*, Leading hadronic contribution to the muon magnetic moment from lattice QCD, Nature (London) **593**, 51 (2021).

[6] R. Aaij *et al.* (LHCb Collaboration), Measurement of the ratio of branching fractions $\mathcal{B}(\bar{B}^0 \to D^{*+}\tau\bar{\nu}_\tau)/\mathcal{B}(\bar{B}^0 \to D^{*+}\mu\bar{\nu}_\mu)$, Phys. Rev. Lett. **115**, 111803 (2015); **115**, 159901(E) (2015).

[7] F. Feruglio, P. Paradisi, and O. Sumensari, Implications of scalar and tensor explanations of $R_{D^{(*)}}$, J. High Energy Phys. 11 (2018) 191.

[8] D. J. Silverman and G. L. Shaw, Limits on the composite structure of the τ lepton and quarks from anomalous magnetic moment measurements in e^+e^- nnihilation, Phys. Rev. D **27**, 1196 (1983).

[9] C. Csaki, C. Delaunay, C. Grojean, and Y. Grossman, A model of lepton masses from a warped extra dimension, J. High Energy Phys. 10 (2008) 055.

[10] M. C. Chen, K. T. Mahanthappa, and F. Yu, A viable Randall-Sundrum model for quarks and leptons with T' family symmetry, Phys. Rev. D **81**, 036004 (2010).

[11] F. del Aguila, A. Carmona, and J. Santiago, Tau custodian searches at the LHC, Phys. Lett. B **695**, 449 (2011).

[12] F. del Aguila, F. Cornet, and J. I. Illana, The possibility of using a large heavy-ion collider for measuring the electromagnetic properties of the tau lepton, Phys. Lett. B **271**, 256 (1991).

[13] A. Kadosh and E. Pallante, An A(4) flavor model for quarks and leptons in warped geometry, J. High Energy Phys. 08 (2010) 115.

[14] The first idea of using photons accompanying fast moving charged particles for physics experiments is due to Enrico Fermi in 1924 [15].

[15] E. Fermi, Sulla teoria dell'urto tra atomi e corpuscoli, Z. Phys. **29**, 315 (1924); **2**, 143 (1925).

[16] DELPHI Collaboration, Study of tau-pair production in photon-photon collisions at LEP and limits on the anomalous electromagnetic moments of the tau lepton, Eur. Phys. J. C **35**, 159 (2004).

[17] G. A. Gonzalez-Sprinberg, A. Santamaria, and J. Vidal, Model independent bounds on the tau lepton electromagnetic and weak magnetic moments, Nucl. Phys. **B582**, 3 (2000).

[18] I. Galon, A. Rajaraman, and T. M. P. Tait, $H \to \tau^+\tau^-\gamma$ as a probe of the τ magnetic dipole moment, J. High Energy Phys. 12 (2016) 111.

[19] U. Haisch, L. Schnell, and J. Weiss, LHC tau-pair production constraints on a_τ and d_τ, SciPost Phys. **16**, 048 (2024).

[20] Lydia Beresford and Jesse Liu, New physics and tau $g-2$ using LHC heavy ion collisions, Phys. Rev. D **102**, 113008 (2020).

[21] Mateusz Dyndal, Mariola Klusek-Gawenda, Matthias Schott, and Antoni Szczurek, Anomalous electromagnetic moment of $\tau - lepton$ in $\gamma\gamma \to \tau^+\tau^-$ reaction in Pb + Pb collisions at the LHC, Phys. Lett. B **809**, 135682 (2020).

[22] CMS Collaboration, Observation of τ lepton pair production in ultraperipheral nucleus-nucleus collisions with the CMS experiment and the first limits on $(g-2)_\tau$ at the LHC, arXiv:2205.05312.

[23] ATLAS Collaboration, Observation of the $\gamma\gamma \to \tau\tau$ process in Pb + Pb collisions and constraints on the τ-lepton anomalous magnetic moment with the ATLAS detector, Phys. Rev. Lett. **131**, 151802 (2023).

[24] X. Chen and Y. Wu, Search for the electric dipole moment and anomalous magnetic moment of the tau lepton at tau factories, J. High Energy Phys. 10 (2019) 089.

[25] A. Crivellin, M. Hoferichter, and J. M. Roney, Toward testing the magnetic moment of the tau at one part per million, Phys. Rev. D **106**, 093007 (2022).

[26] S. Eidelman and M. Passera, Theory of the τ lepton anomalous magnetic moment, Mod. Phys. Lett. A **22**, 159 (2007).

[27] Céline Degrande, Claude Duhr, Benjamin Fuks, David Grellscheid, Olivier Mattelaer, and Thomas Reiter, UFO—The universal FeynRules output, Comput. Phys. Commun. **183**, 1201 (2012).

[28] J. Alwall, M. Herquet, F. Maltoni, O. Mattelaer, and T. Stelzer, MadGraph 5: Going beyond, J. High Energy Phys. 06 (2011) 128.

[29] A. Hoecker *et al.*, TMVA—Toolkit for multivariate data analysis, arXiv:physics/0703039.

[30] D. d'Enterria and J. P. Lansberg, Study of Higgs boson production and its $b-b$ decay in $\gamma-\gamma$ processes in proton-nucleus collisions at the LHC, Phys. Rev. D **81**, 014004 (2010).

[31] C. F. von Weizsacker, Radiation emitted in collisions of very fast electrons, Z. Phys. **88**, 612 (1934).

[32] E. J. Williams, Nature of the high-energy particles of penetrating radiation and status of ionization and radiation formulae, Phys. Rev. **45**, 729 (1934).

[33] J. D. Jackson, *Classical Electrodynamics* (John Wiley & Sons Inc., New York, 1998).

[34] L. A. Harland-Lang, V. A. Khoze, and M. G. Ryskin, Exclusive LHC physics with heavy ions: SuperChic 3, Eur. Phys. J. C **79**, 39 (2019).

[35] V. M. Budnev, I. F. Ginzburg, G. V. Meledin, and V. G. Serbo, The two photon particle production mechanism. Physical problems. Applications. Equivalent photon approximation, Phys. Rep. **15**, 181 (1975).

[36] C. Degrande, C. Duhr, B. Fuks, D. Grellscheid, O. Mattelaer, and T. Reiter, UFO—The Universal FeynRules Output, Comput. Phys. Commun. **183**, 1201 (2012).

[37] A. Alloul, N. D. Christensen, C. Degrande, C. Duhr, and B. Fuks, FeynRules 2.0—A complete toolbox for tree-level phenomenology, Comput. Phys. Commun. **185**, 2250 (2014).

[38] I. Brivio, Y. Jiang, and M. Trott, The SMEFTsim package, theory and tools, J. High Energy Phys. 12 (2017) 070.

[39] T. Sjöstrand , S. Ask, J. R. Christiansen, R. Corke, N. Desai, P. Ilten, S. Mrenna, S. Prestel, C. O. Rasmussen, and P. Z. Skands, An introduction to PYTHIA 8.2, Comput. Phys. Commun. **191**, 159 (2015).

[40] The DELPHES3 Collaboration, DELPHES 3: A modular framework for fast simulation of a generic collider experiment, J. High Energy Phys. 02 (2014) 057.

[41] ATLAS Collaboration, Electron and photon performance measurements with the ATLAS detector using the 2015–2017 LHC proton-proton collision data, J. Instrum. **14**, P12006 (2019).

[42] ATLAS Collaboration, Muon reconstruction and identification efficiency in ATLAS using the full run 2 pp collision data set at $\sqrt{13}$ TeV, Eur. Phys. J. C **81**, 578 (2021).

[43] Alexandre Mertens, New features in DELPHES 3, J. Phys. Conf. Ser. **608**, 012045 (2015).

[44] Michele Selvaggi, DELPHES 3: A modular framework for fast-simulation of generic collider experiments, J. Phys. Conf. Ser. **523**, 012033 (2014).

[45] $\Delta R(\text{lepton-trk}) = \sqrt{(\eta_{\mu,e} - \eta_{\text{trk}})^2 + (\phi_{\text{lepton}} - \phi_{\text{trk}})^2}$ where $\eta_{\text{lepton}}, \phi_{\text{lepton}}$ and $\eta_{\text{trk}}, \phi_{\text{trk}}$ are the pseudorapidities and the azimuthal angles of the lepton and of the track, respectively.

[46] Andreas Hocker *et al.*, TMVA—Toolkit for multivariate data analysis, Report No. CERN-OPEN-2007-007, arXiv: physics/0703039.

[47] K. Choi *et al.*, Towards real-world applications of ServiceX, an analysis data transformation system, EPJ Web Conf. **251**, 02053 (2021).

[48] OPAL Collaboration, An upper limit on the anomalous magnetic moment of the τ lepton, Phys. Lett. B **431**, 188 (1998).

[49] L3 Collaboration, Measurement of the anomalous magnetic and electric dipole moments of the tau lepton, Phys. Lett. B **434**, 169 (1998).